On a negative chemotaxis system with lethal interaction.

Federico Herrero-Hervás[a,*], Mihaela Negreanu[a]

[a]*Departamento de Análisis Matemático y Matemática Aplicada, Instituto de Matemática Interdisciplinar, Universidad Complutense de Madrid, Madrid, Spain*

Abstract

In this work, we propose and analyze a mathematical model describing the interaction between a biological species and a chemical substance through motility, negative chemotaxis, and lethality. The model is based on the interaction of *E. coli* bacteria and hydrogen peroxide (H_2O_2), representing the dual role of H_2O_2: acting as a chemorepellent that causes bacterial cell death while also being produced by the bacteria themselves. The process is modeled using a system of parabolic partial differential equations, which in dimensionless form is given by

$$\begin{cases} u_t = D\Delta u + \chi\nabla\cdot(u\nabla v) + ru(1-u) - uv, & x\in\Omega,\ t>0,\\ \\ v_t = \Delta v + au - v + f(x,t), & x\in\Omega,\ t>0, \end{cases}$$

where u represents the population density of the species, v is the concentration of the substance, f is a source term representing an external supply of the substance and $D,\ \chi,\ r>0$ and $a\geq 0$ are parameters, together with non-negative initial values and Neumann homogeneous boundary conditions.

We first analyze the linear stability of spatially homogeneous steady states for a constant f. For $r<f$, the only biologically relevant state, $(0,f)$ is locally asymptotically stable. Conversely, when $r>f$, a secondary equilibrium state (u_*,v_*) emerges, which is locally asymptotically stable, while $(0,f)$ becomes unstable. The existence of periodic solutions is also investigated when f represents an asymptotically time-periodic supply, deriving a threshold value for r that guarantees its existence.

*Corresponding author

Email addresses: fedher01@ucm.es (Federico Herrero-Hervás), negreanu@mat.ucm.es (Mihaela Negreanu)

Preprint submitted to Commun. Nonlinear Sci. Numer. Simul. *January 12, 2025*

Next, we develop a numerical scheme using the Generalized Finite Difference Method, providing a brief introduction to the method, along with proof of its convergence to the solutions of the system. The work is completed with a numerical study of the analytically studied cases and as well as some final remarks on pattern formation.

Keywords: Chemotaxis, Keller-Segel equations, Periodic Solutions, Generalized Finite Difference Method

1. Introduction

Chemotaxis is a biological phenomenon that allows certain cells and organisms to direct their movements in response to chemical stimuli. Cell receptors allow them to detect concentration gradients of various chemical substances, which can induce either positive or negative chemotaxis, resulting in movement toward or against the highest concentrations of the substance, respectively.

In this paper, we propose and analyze a system of two non-linear parabolic partial differential equations as a model for the dynamics of a bacterial population in competitive interaction with a chemical substance. It is assumed that bacteria move through random diffusion and negative chemotaxis against the concentration of the chemical substance, which is also produced by themselves. A logistic model for bacteria is considered, while in their absence, the substance suffers an exponential decay in time. Moreover, the substance induces cell death in the bacteria and is also externally supplied according to a known source function f.

Such interactions can appear in Nature for instance with *E. coli* bacteria and hydrogen peroxide, H_2O_2. It is known that *E. coli* cells naturally produce between 10 and 15 μM H_2O_2 per second [24, 23], which itself acts as a chemorepellent [7], leading to bacterial death [27] when the concentration can no longer be regulated by their scavenging enzymes (see [15] for an analysis of the effects and killing rate of *E. coli* cells under different exposures to H_2O_2).

Similar scenarios also appear in bacterial species that naturally produce antibiotics, which can at times act against themselves. For instance, *Bacillus subtilis*, responsible for the production of bacilysin, may be susceptible to it under certain mutations, leading to self-inhibition or cell death. A detailed

description on how different antibiotic-producing organisms avoid these self-harms can be found in [8].

We model the process by the following initial-boundary value problem

$$\begin{cases} \dfrac{\partial u}{\partial t} = D_u \Delta u + \chi \nabla \cdot (u \nabla v) + ru\left(1 - \dfrac{u}{K}\right) - \delta uv, & x \in \Omega,\ t > 0, \\ \dfrac{\partial v}{\partial t} = D_v \Delta v + au - bv + f(x,t), & x \in \Omega,\ t > 0, \\ \dfrac{\partial u}{\partial \nu} = \dfrac{\partial v}{\partial \nu} = 0, & x \in \partial\Omega,\ t > 0, \\ u(x,0) = u_0(x), \quad v(x,0) = v_0(x), & x \in \Omega, \end{cases} \tag{1}$$

in a smooth, convex and bounded domain $\Omega \subset \mathbb{R}^n$, where

- u and v respectively represent the densities of the bacterial population and the chemical substance.
- $D_u > 0$, $D_v > 0$ and $\chi > 0$ are the diffusion coefficients of the bacteria and the substance, and the negative chemotaxis sensitivity, respectively.
- $r > 0$, $K > 0$ and $\delta > 0$ are the growth rate of the logistic model, its carrying capacity, and the death rate of the bacteria caused by the substance, respectively.
- $a \geq 0$, $b > 0$ and $f(x,t) \geq 0$ for all $x \in \Omega,\ t > 0$ are the production rate of the substance by the bacteria (the case $a = 0$ corresponds to a scenario where the substance is not secreted by the bacteria, for instance in response to an exogenous antibiotic), the decay rate of the substance, and an external supply of substance, respectively.
- $u_0(x)$ and $v_0(x)$ are the non-negative initial densities.

Historically, systems modeling chemotaxis were first introduced in the works of Keller and Segel [16, 17] in the early 1970s, considering equations

of the form

$$\begin{cases} \dfrac{\partial u}{\partial t} = D_1 \Delta u - \nabla \cdot (\chi u \nabla v) + f(u), & x \in \Omega,\ t > 0, \\ \tau \dfrac{\partial v}{\partial t} = D_2 \Delta v + au - bv, & x \in \Omega,\ t > 0, \end{cases} \tag{2}$$

for positive parameters χ, α, β, a known function f and $\tau \geq 0$. The system (2) was first introduced to model the aggregation process of a slime mold, although many variations have been studied over the years, corresponding to different biological interactions (see, for instance, the surveys [2, 13, 14]).

Competitive dynamics in the form of Lotka-Volterra interaction terms has also been studied within the different variations of chemotaxis models. The following system composed of two competitive species responding to one stimulus that induces positive chemotaxis has been extensively studied.

$$\begin{cases} \dfrac{\partial u}{\partial t} = D_1 \Delta u - \chi_1 \nabla \cdot (u \nabla w) + \mu_1 u(1 - u - a_1 v), & x \in \Omega,\ t > 0, \\ \dfrac{\partial v}{\partial t} = D_2 \Delta v - \chi_2 \nabla \cdot (u \nabla w) + \mu_2 v(1 - a_2 u - v), & x \in \Omega,\ t > 0, \\ \tau \dfrac{\partial w}{\partial t} = D_3 \Delta w - \gamma w + \alpha u + \beta v, & x \in \Omega,\ t > 0, \end{cases} \tag{3}$$

The parabolic case (for $\tau = 1$) was analyzed by Bai and Winkler in [1], where the global existence of solutions for $n \leq 2$ was proven under certain restrictions for μ_1 and μ_2. The large time convergence of solutions to its spatially homogeneous steady states was also studied. These results were improved later in [19], with lighter restrictions on μ_1 and μ_2. The higher dimensional case was analyzed in [29]

Respectively, the elliptic case has been studied in [26] for the weakly competitive case ($0 < a1, a_2 < 1$) with similar restrictions for the convergence regarding μ_1, μ_2 and χ_1, χ_2 leading to the convergence to its spatially homogeneous steady states. In [25] a competitive exclusion result is obtained.

In this paper, however, we consider just one species, with the competitive term appearing only in the first equation of (1), representing the cell death caused by the chemical. As previously stated, the model is based on the dynamics naturally appearing in *E. coli* bacteria and H_2O_2.

After rescaling the variables by considering

$$\tilde{u} = \frac{u}{K},\ \tilde{v} = \frac{\delta K}{b} v,\ \tilde{x} = \sqrt{\frac{b}{D_v}} x,\ \tilde{t} = bt,$$

and the dimensionless parameters

$$D = \frac{D_u}{D_v},\ \tilde{\chi} = \frac{b\chi}{\delta K D_v},\ \tilde{r} = \frac{r}{b},\ \tilde{a} = \frac{a\delta K^2}{b^2},\ \tilde{f} = \frac{\delta K}{b^2} f,$$

we obtain the following system, after dropping the tildes.

$$\begin{cases} \dfrac{\partial u}{\partial t} = D\Delta u + \chi \nabla \cdot (u \nabla v) + ru(1-u) - uv, & x \in \Omega,\ t > 0, \\ \dfrac{\partial v}{\partial t} = \Delta v + au - v + f(x,t), & x \in \Omega,\ t > 0, \\ \dfrac{\partial u}{\partial \nu} = \dfrac{\partial v}{\partial \nu} = 0, & x \in \partial\Omega,\ t > 0, \\ u(x,0) = u_0(x), \quad v(x,0) = v_0(x), & x \in \Omega. \end{cases} \tag{4}$$

Throughout this paper, we study the local stability of the spatially homogeneous steady states of system (4) when f is a constant supply, as well as the periodicity of solutions for a time periodic source f.

For a constant f, the system admits two spatially homogeneous steady states, given by

$$(0, f), \quad (u_*, v_*) := \left(\frac{r-f}{r+a}, \frac{r(f+a)}{r+a} \right).$$

Notice that (u_*, v_*) is only biologically relevant if $r > f$, this is, in the case where the bacterial growth rate is greater than the external supply of the substance. On the contrary, whenever $r < f$, the only nonnegative equilibrium is given by $(0, f)$. The linearized dynamics and local stability of these solutions is studied in Section 2.

The case where f converges to a time-periodic function is studied in Section 3. We specifically consider f to have a periodic asymptotic behavior

in the sense that there exists a time periodic function $\hat{f} : (0, +\infty) \to \mathbb{R}$, only dependent of t such that

$$\lim_{t \to +\infty} \sup_{x \in \Omega} |f(x,t) - \hat{f}(t)| = 0, \quad \forall x \in \Omega.$$

The associated ODE system

$$\begin{cases} \tilde{u}_t = r\tilde{u}(1-\tilde{u}) - \tilde{u}\tilde{v}, & t > 0, \\ \\ \tilde{v}_t = -\tilde{v} + \hat{f}(t), & t > 0, \end{cases} \tag{5}$$

is proven to admit a positive periodic solution for $a = 0$ (when the substance is not produced by the bacteria) if a threshold value for r is exceeded. Moreover, numerical experiments performed later on in the article also allow us to obtain periodic solutions when $a > 0$. The periodicity is then inherited by the PDE system, with its solutions (u, v) converging in time to the solutions $(\tilde{u}, \tilde{v})$ of the ODE system at all $x \in \Omega$.

For the numerical study, we make use of the Generalized Finite Difference (GFD) Method, a meshless method which has been successfully applied to numerous nonlinear problems. Precisely within the numerical analysis of chemotaxis systems, the authors in [4, 5, 6, 10, 11] study a wide range of extensions of the Keller-Segel model, corresponding to parabolic-parabolic, parabolic-elliptic and parabolic-ODE problems. In our case, after an introduction of the method in Section 4, in Section 5 we derive conditions for the convergence of an explicit scheme for computing the numerical solution to system (4). Numerical simulations are performed in Section 6 to illustrate the cases studied analytically regarding the local stability and periodicity, as well as a brief subsection regarding pattern formation in the system. Lastly, the conclusions are collected in Section 7.

2. Linearized dynamics and local stability

To begin the analysis of system (4), we study the local stability of its spatially homogeneous steady states, which are obtained by solving

$$\begin{cases} 0 = ru(1-u-v), \\ \\ 0 = au - v + f(x,t). \end{cases}$$

Such solutions can only exist for a constant source $f(x,t) \equiv f$, resulting in two values

$$(0, f), \quad (u_*, v_*) := \left(\frac{r-f}{r+a}, \frac{r(f+a)}{r+a} \right). \tag{6}$$

For a biological interpretation, we require that both u and v are non-negative, and thus (u_*, v_*) is only meaningful if $r > f$, corresponding to a bacterial growth rate greater than the external supply of the substance.

To assess the local stability of these points, we make use of the principle of linearized stability for quasilinear parabolic problems, [9]. Letting $\bar{u}$, $\bar{v}$ denote any of the previous spatially homogeneous steady states, we consider perturbed solutions of the form

$$u = \bar{u} + \varepsilon\phi, \quad v = \bar{v} + \varepsilon\eta \tag{7}$$

for $0 < \varepsilon \ll 1$. By substituting (7) in system (4) and neglecting the terms of order ε^2, we arrive at the linearized system that ϕ and η solve, which is given by

$$\begin{cases} \dfrac{\partial \phi}{\partial t} = D\Delta\phi + \chi\bar{u}\Delta\eta - [(1-2\bar{u})r - \bar{v}]\phi - \bar{u}\eta, & x \in \Omega,\ t > 0, \\ \\ \dfrac{\partial \eta}{\partial t} = \Delta\eta + a\phi - \eta, & x \in \Omega,\ t > 0, \end{cases} \tag{8}$$

together with Neumann homogeneous boundary conditions and their respective initial values. System (8) can be re-expressed as

$$\begin{pmatrix} \phi_t \\ \eta_t \end{pmatrix} = \boldsymbol{D} \cdot \begin{pmatrix} \Delta\phi \\ \Delta\eta \end{pmatrix} + \boldsymbol{J} \cdot \begin{pmatrix} \phi \\ \eta \end{pmatrix} =: L \begin{pmatrix} \phi \\ \eta \end{pmatrix}, \tag{9}$$

where

$$\boldsymbol{D} = \begin{pmatrix} D & \chi\bar{u} \\ 0 & 1 \end{pmatrix}, \quad \boldsymbol{J} = \begin{pmatrix} (1-2\bar{u})r - \bar{v} & -\bar{u} \\ a & -1 \end{pmatrix}.$$

The stability of the points $(\bar{u}, \bar{v})$ is given by the eigenvalue problem

$$L \begin{pmatrix} \phi \\ \eta \end{pmatrix} = \mu \begin{pmatrix} \phi \\ \eta \end{pmatrix},$$

which, though considering the sequence of eigenvalues

$$0 = \lambda_0 < \lambda_1 \leq \lambda_2 \leq \ldots, \quad \text{with } \lim_{n\to\infty} \lambda_n = +\infty$$

of the operator $-\Delta$ with Neumann boundary conditions defined on the space

$$S = \{\varphi \in W^{2,p}(\Omega),\ \frac{\partial \varphi}{\partial \nu} = 0 \text{ in } \partial\Omega\},$$

is equivalent to studying the eigenvalues of the matrix $\boldsymbol{A}_n := -\lambda_n \boldsymbol{D} + \boldsymbol{J}$ for all $n \in \{0, 1, 2, \dots\}$. A spatially homogeneous steady state $(\bar{u}, \bar{v})$ is locally asymptotically stable if and only if all the eigenvalues of $\boldsymbol{A}_n$ have negative real part for all $n \in \{0, 1, 2, \dots\}$. On the contrary, if there exists n such that $\boldsymbol{A}_n$ has at least one eigenvalue with positive real part, then $(\bar{u}, \bar{v})$ is unstable.

Next, we perform the computations for our two points, $(0, f)$ and (u_*, v_*). Firstly, for $(\bar{u}, \bar{v}) = (0, f)$, we obtain

$$\boldsymbol{A}_n = \begin{pmatrix} -\lambda_n D + r - f & 0 \\ a & -\lambda_n - 1 \end{pmatrix},$$

whose eigenvalues are trivially given by $\mu_{n_1} = -\lambda_n D + r - f$ and $\mu_{n_2} = -\lambda_n - 1$. Taking into account that $0 = \lambda_0 < \lambda_1 \leq \lambda_2 \leq \dots$, we directly have that $\mu_{n_2} < 0$ for all $n \in \{0, 1, 2, \dots\}$. With respect to μ_{n_1}, as $\lambda_0 = 0$, it follows that for $n = 0$, $\mu_{0_1} < 0$ if and only if $r < f$. For $n \geq 1$, as the sequence λ_n is increasing, $\mu_{n_1} < \mu_{n_0}$. Therefore, we conclude that $(0, f)$ is locally asymptotically stable if and only if $r < f$. For $r > f$, the point is unstable.

For $(\bar{u}, \bar{v}) = (u_*, v_*) = \left(\dfrac{r-f}{r+a}, \dfrac{r(f+a)}{r+a}\right)$, $\boldsymbol{A}_n$ is given by

$$\boldsymbol{A}_n = \begin{pmatrix} -\lambda_n D + \dfrac{r(f-r)}{r+a} & \dfrac{f-r}{r+a}(\lambda_n \chi + 1) \\ a & -\lambda_n - 1 \end{pmatrix}$$

Recall that (u_*, v_*) is only biologically relevant if $r > f$, which is the only case in which we perform the stability analysis. The characteristic polynomial of $\boldsymbol{A}_n$ is

$$\begin{aligned} \mathcal{P}_{\boldsymbol{A}_n}(\mu) = \mu^2 - \left(-\lambda_n D + \frac{r(f-r)}{r+a} - \lambda_n - 1\right)\mu \\ - a\frac{f-r}{r+a}(\lambda_n \chi + 1) - (\lambda_n + 1)\left(-\lambda_n D + \frac{r(f-r)}{r+a}\right). \end{aligned}$$

In the case of a 2×2 matrix $\boldsymbol{A}$ with eigenvalues $\mu_1,\ \mu_2$, its characteristic polynomial satisfies $\mathcal{P}_{\boldsymbol{A}}(\mu) = \mu^2 - \mathrm{tr}(\boldsymbol{A})\mu + \det(\boldsymbol{A}) = \mu^2 - (\mu_1+\mu_2)\mu + \mu_1\mu_2$.

Denoting again by $\mu_{n_1},\ \mu_{n_2}$ the two eigenvalues of $\boldsymbol{A}_n$ for every n, we thus have

$$\mathrm{tr}(\boldsymbol{A}_n) = \mu_{n_1} + \mu_{n_2} = -\lambda_n D + \frac{r(f-r)}{r+a} - \lambda_n - 1,$$
$$\det(\boldsymbol{A}_n) = \mu_{n_1}\mu_{n_2} = -a\frac{f-r}{r+a}(\lambda_n\chi + 1) - (\lambda_n + 1)\left(-\lambda_n D + \frac{r(f-r)}{r+a}\right).$$

Given that we are only interested in the case $r > f$, clearly $\mu_{n_1} + \mu_{n_2} < 0$ and $\mu_{n_1}\mu_{n_2} > 0$, which means that the point is locally asymptotically stable.

Overall this means:

- If $r < f$, the only non-negative spatially homogeneous steady state is $(0, f)$, which is locally asymptotically stable.
- If $r > f$, both spatially homogeneous steady states, $(0, f)$ and (u_*, v_*), are biologically meaningful. The first one is unstable, while the second one is locally asymptotically stable.

From a biological point of view, if $r < f$ —this is, if the growth rate of the bacteria is less than the external supply of the chemorepellent—, then $(0, f)$ is the only existing equilibrium and is locally asymptotically stable. Hence, for $u(x, 0)$ close to zero, the solution u ends up converging to zero, as the intrinsic bacterial growth is not large enough to compensate the death term $-uv$, as v is growing faster due to the largeness of f.

On the contrary, if $r > f$, the point $(0, f)$ is unstable, as the logistic growth exceeds the external supply of the substance. The other spatially homogeneous steady state, (u_*, v_*) of coexistence of the bacteria and the species, is locally asymptotically state. Here, despite the growth being greater than the supply, both u and v are large enough for $-uv$ to be significant.

Notice that these behaviors are independent of the remaining parameters, D, χ and a, meaning that the linearized dynamics of the system are governed only by the balance between the source term f and the logistic growth rate r.

3. Periodic solutions

Now, we investigate the existence of periodic solutions to our system (4). In this case, we consider a source f with asymptotic periodic behavior. More

precisely, we assume that there exists a function $\hat{f} : (0, +\infty) \to \mathbb{R}$ that only depends on time and is periodic with period $T > 0$, such that

$$\lim_{t \to +\infty} \sup_{x \in \Omega} |f(x,t) - \hat{f}(t)| = 0, \quad \forall x \in \Omega.$$

This is the same requirement established in other similar articles such as [20, 21]. Here we prove that, under suitable hypotheses, the solution of system (4) converges to the periodic solution of the associated ODE system (5).

We first analyze the case $a = 0$, which occurs when the substance is not produced by the bacteria, which for instance occurs in a bacterial response to a supply of exogenous antibiotics. Note than in this case, the associated ODE system is given by

$$\begin{cases} \tilde{u}_t = r\tilde{u}(1 - \tilde{u}) - \tilde{u}\tilde{v}, & t > 0, \\ \\ \tilde{v}_t = -\tilde{v} + \hat{f}(t), & t > 0, \end{cases} \tag{10}$$

where the second equation is uncoupled and linear. We can use this to explicitly derive conditions on the initial values $(\tilde{u}_0, \tilde{v}_0)$ for the solution to be periodic. Solving the second equation leads to

$$\tilde{v}(t) = e^{-t} \left[\tilde{v}_0 + \int_0^t \hat{f}(s) e^s \, ds \right]. \tag{11}$$

For the solution to have the same periodicity as $\hat{f}$, we require that $\tilde{v}(t) = \tilde{v}(t + T)$ or equivalently, as $\hat{f}$ is periodic, $\tilde{v}(T) = \tilde{v}_0$. Thus

$$\tilde{v}_0 = \tilde{v}(T) = e^{-T} \left[\tilde{v}_0 + \int_0^T \hat{f}(s) e^s \, ds \right].$$

Therefore, the condition for $\tilde{v}$ to be periodic is that $\tilde{v}(0)$ is such that

$$\tilde{v}_0 = \frac{1}{e^T - 1} \int_0^T \hat{f}(s) e^s \, ds. \tag{12}$$

For $\tilde{u}$, we can proceed similarly. Rewriting the equation as

$$\tilde{u}_t = (r - \tilde{v})\tilde{u} - r\tilde{u}^2,$$

we clearly see that it is a Bernoulli ODE, which can again the explicitly solved. By considering $\tilde{w} = \tilde{u}^{-1}$, we have $w_t = -\tilde{u}_t\ \tilde{u}^{-2}$, where the equation satisfied by $\tilde{w}$ is linear, given by

$$\tilde{w}_t + (r - \tilde{v})\tilde{w} = r, \quad \tilde{w}(0) = 1/\tilde{u}_0 =: \tilde{w}_0, \tag{13}$$

where we can follow the previous steps, as $\tilde{v}$ is periodic, provided $\tilde{v}_0$ satisfies (12). Explicitly solving (13) we have

$$\tilde{w}(t) = e^{-\int_0^t (r - \tilde{v}(s))\ ds} \left[\tilde{w}_0 + \int_0^t \left(r\ e^{\int_0^s (r - \tilde{v}(\tau))\ d\tau} \right)\ ds \right], \tag{14}$$

and in turn $\tilde{u}$ is periodic if $\tilde{u}(T) = \tilde{u}_0$ or equivalently $\tilde{w}(T) = \tilde{w}_0$. This results in the following condition for the periodicity of $\tilde{u}$.

$$\tilde{u}_0 = \frac{e^{\int_0^T (r - \tilde{v}(s))\ ds} - 1}{\int_0^T \left(r\ e^{\int_0^s (r - \tilde{v}(\tau))\ d\tau} \right)\ ds}. \tag{15}$$

Therefore, for the solution $(\tilde{u}, \tilde{v})$ to be periodic with the same period as f, both $\tilde{u}_0$ and $\tilde{v}_0$ have to satisfy (15) and (12), respectively. An important bound can be derived for (15). For the biological relevance of the system, only positive solutions are considered, therefore $\tilde{v}$ must satisfy

$$e^{\int_0^T (r - \tilde{v}(s))\ ds} - 1 > 0,$$

or equivalently

$$r > \frac{1}{T} \int_0^T \tilde{v}(s)\ ds. \tag{16}$$

Notice that this is a bound for r with respect to the choice of f, as $\tilde{v}$ is independent from r. Thus, there exists a threshold given by the average value of $\tilde{v}$,

$$r_{\min} = \frac{1}{T} \int_0^T \tilde{v}(s)\ ds, \tag{17}$$

which makes $\tilde{u}_0$ positive. If $r > r_{\min}$ and $(\tilde{u}_0, \tilde{v}_0)$ are taken as in (15) and (12), respectively, then the unique solution $(\tilde{u}, \tilde{v})$ of system (10) is periodic and positive. If on the contrary $r < r_{\min}$, no solution with such properties can exist.

An explicit formula for $r_{\min}$ depending only on $\hat{f}$ can be obtained substituting in (17) the expression for $\tilde{v}$ given in (11). Integrating by parts and using the value of $\tilde{v}_0$ from (12), this directly yields

$$r_{\min} = \frac{1}{T} \int_0^T \hat{f}(s)\ ds. \tag{18}$$

Again, similarly as what we obtained for the local stability with constant f, the periodicity of the associated ODE system lies on a threshold phenomena with respect to r and, in this case, $\hat{f}$. This exhibits an analogy with the case $r > f$ with constant f, for which (u_*, v_*) was locally asymptotically stable. Biologically, these periodic dynamics can only occur if again the logistic growth rate of the species is large enough with respect to the external periodic source.

Periodic solutions to the ODE system in the case $a > 0$ have only been studied numerically at the moment, detailed in the corresponding Section 6.3, though the analytical part is still work in progress. It is proven in [12] that under the previous hypotheses, the solution to (u, v) of the full PDE system (4) converges in time to $(\tilde{u}, \tilde{v})$ for all $x \in \Omega$.

4. Preliminaries for the numerical method

In this section we explain the procedure to obtain the discretization of the partial derivatives of a function in terms of its values over a set of arbitrary nodes, which characterize this meshless method. Let Ω be a domain in $\mathbb{R}^2$ and $M = \{x_1, x_2, ...x_N\}$ a discretization of such domain, where we seek to approximate the partial derivatives of the function. For the ease of notation and, without loss of generality, let us consider a set of s different points of M, say $V = \{x_1, x_2, ..., x_s\}$, and denote a generic interior point of $M - V$ as x_0, where we derive the approximation. There are different criteria such as distance, quadrant or octant criteria can be used to select these s nodes, that make up what is known as an E_s-star. In order to obtain the equation of the star for each of the these points, we look at the truncated second order Taylor series expansion at $\mathbf{x}_0$ of the function f where $f(\mathbf{x}_i, n\Delta t) = f_i^n$

(although we omit the time dependence since it is not necessary now) is the approximation of the continuous solution of the problem,

$$F_i \approx F_0 + (\mathbf{x}_i - \mathbf{x}_0)\nabla F_0 + \frac{1}{2}(\mathbf{x}_i - \mathbf{x}_0)^T H_{F_0}(\mathbf{x}_i - \mathbf{x}_0). \tag{19}$$

We define now the vectors $\mathbf{d} = \left(\frac{\partial F_0}{\partial x}, \frac{\partial F_0}{\partial y}, \frac{\partial^2 F_0}{\partial x^2}, \frac{\partial^2 F_0}{\partial y^2}, \frac{\partial^2 F_0}{\partial x \partial y}\right)$, which contains the partial derivatives that we want to approximate, and $\mathbf{c}_i = \left(h_i, k_i, \frac{h_i^2}{2}, \frac{k_i^2}{2}, h_i k_i\right)$, where as usual, we take $h_i = x_i - x_0$ and $k_i = y_i - y_0$. Let us define the sum of the weighted quadratic errors as the operator B

$$B(\mathbf{d}) = \sum_{i=1}^{s} (F_0 - F_i + \mathbf{c}_i^T \mathbf{d})^2 w_i^2 + \mathcal{O}(h_i^2, k_i^2),$$

where $w_i = w(h_i, k_i)$ are positive symmetrical weighting functions and decreasing in magnitude as the distance to the center increases, as defined in Lancaster and Salkauskas [18]. Some weighting functions as potentials ($\frac{1}{\text{dist}^4}$ or $\frac{1}{\text{dist}^6}$) or exponential, $e^{-\text{dist}^2}$, can be used (more details can be found in [28]). By minimizing B with respect to $\mathbf{d}$, the following linear system is achieved

$$\sum_{i=1}^{s} w_i^2 \mathbf{c}_i \mathbf{c}_i^T \mathbf{d} = -\sum_{i=1}^{s} w_i^2 (F_0 - F_i)\mathbf{c}_i.$$

Let us define $A := \sum_{i=1}^{s} w_i^2 \mathbf{c}_i \mathbf{c}_i^T$, that is,

$$\boldsymbol{A} = \begin{pmatrix} h_1 & h_2 & \cdots & h_s \\ k_1 & k_2 & \cdots & k_s \\ \vdots & \vdots & \vdots & \vdots \\ h_1 k_1 & h_2 k_2 & \cdots & h_s k_s \end{pmatrix} \begin{pmatrix} \omega_1^2 & & & \\ & \omega_2^2 & & \\ & & \cdots & \\ & & & \omega_s^2 \end{pmatrix} \begin{pmatrix} h_1 & k_1 & \cdots & h_1 k_1 \\ h_2 & k_2 & \cdots & h_2 k_2 \\ \vdots & \vdots & \vdots & \vdots \\ h_s & k_s & \cdots & h_s k_s \end{pmatrix} \tag{20}$$

Properties of $\mathbf{A}$ are well-known, as can be consulted in [28]. In particular, it is positive definite and, therefore,

$$\mathbf{d} = -F_0 \sum_{i=1}^{s} w_i^2 A^{-1} \mathbf{c}_i + \sum_{i=1}^{s} F_i w_i^2 A^{-1} \mathbf{c}_i + \mathcal{O}(h_i^2, k_i^2).$$

For simplicity, we write

$$\boldsymbol{m}_0 = \sum_{i=1}^{s} w_i^2 \mathbf{A}^{-1}\mathbf{c}_i, \quad \boldsymbol{m}_i = w_i^2 \mathbf{A}^{-1}\mathbf{c}_i.$$

Then, introducing the notation $\boldsymbol{m}_0 = (m_{01}, m_{02}, m_{03}, m_{04}, m_{05})^T$ (and similarly for $\boldsymbol{m}_i$), we express the partial derivatives of the function as a linear combination of the approximated values of f in the points of the star:

$$\begin{cases} \dfrac{\partial F(\mathbf{x}_0, n\Delta t)}{\partial x} = -m_{01}F_0^n + \displaystyle\sum_{i=1}^{s} m_{i1}F_i^n + \mathcal{O}(h_i^2, k_i^2), \\ \dfrac{\partial F(\mathbf{x}_0, n\Delta t)}{\partial y} = -m_{02}F_0^n + \displaystyle\sum_{i=1}^{s} m_{i2}F_i^n + \mathcal{O}(h_i^2, k_i^2), \\ \dfrac{\partial^2 F(\mathbf{x}_0, n\Delta t)}{\partial x^2} + \dfrac{\partial^2 F(\mathbf{x}_0, n\Delta t)}{\partial y^2} = -(m_{03} + m_{04})F_0^n + \displaystyle\sum_{i=1}^{s}(m_{i3} + m_{i4})F_i^n \\ \qquad\qquad := -m_{00}F_0 + \displaystyle\sum_{i=1}^{s} m_{i0}F_i + \mathcal{O}(h_i^2, k_i^2). \end{cases} \tag{21}$$

The time derivative approximation is computed with the classical forward difference formula, of first order,

$$\frac{\partial F(\mathbf{x}_0, n\Delta t)}{\partial t} = \frac{F_0^{n+1} - F_0^n}{\Delta t} + \mathcal{O}(\Delta t). \tag{22}$$

5. Numerical scheme and convergence

Let $\Omega \subset \mathbb{R}^2$ be a bounded and convex domain. By using the formulae (22) for the approximation of the spatial derivatives and the time derivative approximation

$$\frac{\partial u(x_0, y_0, n\Delta t)}{\partial t} = \frac{u_0^{n+1} - u_0^n}{\Delta t} + \mathcal{O}(\Delta t), \tag{23}$$

we obtain the following 2-dimensional GFD explicit scheme:

$$\begin{cases} u_0^{n+1} = u_0^n + \Delta t \left[D\left(-m_{00}u_0^n + \sum_{i=1}^{s} m_{0i}u_i^n \right) - \chi u_0^n \left(-m_{00}v_0^n + \sum_{i=1}^{s} m_{0i}v_i^n \right) \right] \\ \qquad + \chi \Delta t \left(-m_{01}u_0^n + \sum_{i=1}^{s} + m_{i1}u_i^n \right) \left(-m_{01}v_0^n + \sum_{i=1}^{s} + m_{i1}v_i^n \right) \\ \qquad + \chi \Delta t \left(-m_{02}u_0^n + \sum_{i=1}^{s} + m_{i2}u_i^n \right) \left(-m_{02}v_0^n + \sum_{i=1}^{s} + m_{i2}v_i^n \right) \\ \qquad + \Delta t \cdot r u_0^n \left[1 - u_0^n \right] - \Delta t u_0^n v_0^n + \mathcal{O}(\Delta t, h_i^2, k_i^2) \\ v_0^{n+1} = v_0^n \left[1 - \Delta t(1 + m_{00}) \right] + \Delta t \cdot a u_0^n + \Delta t \sum_{i=1}^{s} m_{0i}v_i^n + f_0^n + \mathcal{O}(\Delta t, h_i^2, k_i^2). \end{cases} \tag{24}$$

In order to prove the convergence of the method, we need some basic results which we enunciate for completeness:

Lemma 5.1. *Let be a matrix $\mathcal{N} \in \mathfrak{M}_{n\times n}(\mathbb{R})$. If there exists some matrix norm verifying $\|\mathcal{N}\| < 1$, then*

$$\lim_{k\to\infty} \mathcal{N}^k = \boldsymbol{0}.$$

Lemma 5.2. *Assume $\mathcal{N} \in \mathfrak{M}_{n\times n}(\mathbb{R})$, then the following issues are equivalent:*

(i) $\lim_{k\to\infty} \mathcal{N}^k = \boldsymbol{0}$,

(ii) $\rho(\mathcal{N}) < 1$,

where $\rho(\cdot)$ stands for the spectral radius.

For the sake of simplicity, let us name some of the expressions which appear in the proof of the conditional convergence of the scheme:

$$\begin{aligned} A_1 := \Bigg[\Bigg| & \chi(m_{01})^2 V_0^n + \chi(m_{02})^2 V_0^n - \\ & - \chi\left(m_{01} \sum_{i=1}^{s} m_{i1} V_i^n + m_{02} \sum_{i=1}^{n} m_{i2} V_i^n \right) \\ & - (\chi - \mu)(u_0^n + U_0^n) + \chi V_0^n - \mu(1 + f(x_0, y_0, n\Delta t)) \Bigg| \\ & + |\chi m_{01} v_0^n| \sum_{i=1}^{s} |m_{i1}| + |\chi m_{02} v_0^n| \sum_{i=1}^{s} |m_{i2}| \\ & + |\chi \sum_{i=1}^{s} m_{i1} V_i^n| \sum_{i=1}^{s} |m_{i1}| + |\chi \sum_{i=1}^{s} m_{i2} V_i^n| \sum_{i=1}^{s} |m_{i2}| \Bigg], \end{aligned} \tag{25}$$

$$\begin{aligned} B_1 := \Bigg[\Bigg| & \chi[-(m_{01})^2 - (m_{02})^2] u_0^n + \chi m_{01} \sum_{i=1}^{s} m_{i1} u_i^n \\ & + \chi m_{02} \sum_{i=1}^{s} m_{i2} u_0^n - \chi u_0^n \Bigg| + |\chi m_{01} U_0^n| \sum_{i=1}^{s} |m_{i1}| \\ & + |\chi m_{02} U_0^n| \sum_{i=1}^{s} |m_{i2}| + \chi| \sum_{i=1}^{s} m_{i1} U_i^n| \sum_{i=1}^{s} |m_{i1}| \\ & + \chi| \sum_{i=1}^{s} m_{i2} U_i^n| \sum_{i=1}^{s} |m_{i2}| \Bigg], \end{aligned} \tag{26}$$

Theorem 5.1. *Let $U, V \in \mathcal{C}^4(\Omega_\infty)$ be the exact solution of (1). Then, the GFD explicit scheme (24) is convergent if*

$$\Delta t < \min \left\{ \frac{2}{m_{00} + \sum_{i=1}^{s} |m_{i0}| + A_1 + B_1}, \frac{2}{1 + m_{00} + \sum_{i=1}^{s} |m_{i0}| + \Delta t a} \right\}, \tag{27}$$

where A_1 and B_1 are explicitly shown in the proof.

Proof of Theorem 5.1
We take the difference between GFD scheme (24) and the expression for the exact solution. Let u_j^n be the approximated u-solution at time $n\Delta t$ (similarly v_j^n) and U_j^n the value of the exact U-solution (similarly V_j^n). Also, we call $\tilde{u}_j^n = u_j^n - U_j^n$, $\tilde{v}_j^n = v_j^n - V_j^n$. The following expression yields

$$\begin{aligned}
\tilde{u}_0^{n+1} =& \tilde{u}_0^n + D\Delta t\left(-m_{00}\tilde{u}_0^n + \sum_{i=1}^{s} m_{i0}\tilde{u}_i^n\right) \\
&+ \chi\Delta t\left[\left(-m_{01}u_0^n + \sum_{i=1}^{s} m_{i1}u_i^n\right)\left(-m_{01}v_0^n + \sum_{i=1}^{s} m_{i1}v_i^n\right)\right. \\
&\left. - \left(-m_{01}U_0^n + \sum_{i=1}^{s} m_{i1}U_i^n\right)\left(-m_{01}V_0^n + \sum_{i=1}^{s} m_{i1}V_i^n\right)\right] \\
&+ \chi\Delta t\left[\left(-m_{02}u_0^n + \sum_{i=1}^{s} m_{i2}u_i^n\right)\left(-m_{02}v_0^n + \sum_{i=1}^{s} m_{i2}v_i^n\right)\right. \\
&\left. - \left(-m_{02}U_0^n + \sum_{i=1}^{s} m_{i2}U_i^n\right)\left(-m_{02}V_0^n + \sum_{i=1}^{s} m_{i2}V_i^n\right)\right] \\
&- \Delta t\chi m_{00}[\tilde{u}_0^n v_0^n + U_0^n\tilde{v}_0^n] + \Delta t\chi\left(\tilde{u}_0^n\sum_{i=1}^{s} m_{i0}v_i^n + U_0^n\sum_{i=1}^{s} m_{i0}\tilde{v}_i^n\right) \\
&- \Delta t r\tilde{u}_0^n[1 - (u_0^n + U_0^n)] - \Delta t\tilde{u_0^n}v_0^n - \Delta t U_0^n\tilde{v}_0^n + \mathcal{O}(\Delta t(\Delta t, h_i^2, k_i^2)).
\end{aligned} \tag{28}$$

After some direct computations and taking bounds, it yields

$$
\begin{aligned}
\tilde{u}_0^{n+1} = \tilde{u}_0^n \Bigg[& 1 - Dm_{00}\Delta t + \Delta t\chi(m_{01})^2 V_0^n + \Delta t\chi(m_{02})^2 V_0^n \\
& - \Delta t\chi\left(m_{01}\sum_{i=1}^{s} m_{i1}v_i^n + m_{02}\sum_{i=1}^{n} m_{i2}v_i^n \right) + \Delta t\chi \sum_{i=1}^{s} m_{i0}v_i^n \\
& - \Delta t\chi m_{00}v_0^n - \Delta t r[1-(u_0^n + U_0^n)] - \Delta t v_0^n \Bigg] \\
& + \Delta t \Bigg[D\sum_{i=1}^{s} m_{i0}\tilde{u}_i^n - \chi m_{01}V_0^n \sum_{i=1}^{s} m_{i1}\tilde{u}_i^n - \chi m_{02}V_0^n \sum_{i=1}^{s} m_{i2}\tilde{u}_i^n \\
& + \left(\chi \sum_{i=1}^{s} m_{i1}v_i^n \right) \sum_{i=1}^{s} m_{i1}\tilde{u}_i^n + \left(\chi \sum_{i=1}^{s} m_{i2}v_i^n \right) \sum_{i=1}^{s} m_{i2}\tilde{u}_i^n \Bigg] \\
& + \Delta t\tilde{v}_0^n \Bigg[\left(\chi(m_{01})^2 + \chi(m_{02})^2 \right) U_0^n - \chi m_{01} \sum_{i=1}^{s} m_{i1}u_i^n \\
& - \chi m_{02} \sum_{i=1}^{s} m_{i2}u_i^n - \chi m_{00}U_0^n - U_0^n \Bigg] \\
& + \Delta t \Bigg[-\chi m_{01}U_0^n \sum_{i=1}^{s} m_{i1}\tilde{v}_i^n - \chi m_{02}U_0^n \sum_{i=1}^{s} m_{i2}\tilde{v}_i^n \\
& + \chi \left(\sum_{i=1}^{s} m_{i1}U_i^n \right) \sum_{i=1}^{s} m_{i1}\tilde{v}_i^n + \chi \left(\sum_{i=1}^{s} m_{i2}U_i^n \right) \sum_{i=1}^{s} m_{i2}\tilde{v}_i^n \Bigg] \\
& + \mathcal{O}(\Delta t(\Delta t, h_i^2, k_i^2)).
\end{aligned}
\tag{29}
$$

Let us define $\tilde{u}^n = \max_{i\in\{0,\dots,s\}} |\tilde{u}_i^n|$ and $\tilde{v}^n = \max_{i\in\{0,\dots,s\}} |\tilde{v}_i^n|$. We rewrite

(29) as follows

$$\begin{aligned}
\tilde{u}^{n+1} \leq \tilde{u}^n \Bigg[\Bigg| 1 - \Delta t \Bigg(& D m_{00} - \chi (m_{01})^2 V_0^n - \chi (m_{02})^2 V_0^n \\
& + \chi \left(m_{01} \sum_{i=1}^{s} m_{i1} v_i^n + m_{02} \sum_{i=1}^{n} m_{i2} v_i^n \right) - \chi \sum_{i=1}^{s} m_{i0} v_i^n \\
& + \chi m_{00} v_0^n + r[1 - (u_0^n + U_0^n)] + v_0^n \Bigg) \Bigg| \\
& + \Delta t D \sum_{i=1}^{s} |m_{i0}| + \chi |m_{01} V_0^n \sum_{i=1}^{s} m_{i1}| + \chi |m_{02} V_0^n \sum_{i=1}^{s} m_{i2}| \\
& + \left| \chi \sum_{i=1}^{s} m_{i1} v_i^n \right| \sum_{i=1}^{s} |m_{i1}| + \left| \chi \sum_{i=1}^{s} m_{i2} v_i^n \right| \sum_{i=1}^{s} |m_{i2}| \Bigg] \\
& + \Delta t \tilde{v} \Bigg[\Bigg| (\chi (m_{01})^2 + \chi (m_{02})^2) U_0^n - \chi m_{01} \sum_{i=1}^{s} m_{i1} u_i^n \\
& - \chi m_{02} \sum_{i=1}^{s} m_{i2} u_i^n - \chi m_{00} U_0^n - U_0^n \Bigg| + \chi |m_{01} U_0^n \sum_{i=1}^{s} m_{i1}| \\
& + \chi |m_{02} U_0^n \sum_{i=1}^{s} m_{i2}| + \chi \left| \sum_{i=1}^{s} m_{i1} U_i^n \right| \sum_{i=1}^{s} |m_{i1}| \\
& + \chi \left| \sum_{i=1}^{s} m_{i2} U_i^n \right| \sum_{i=1}^{s} |m_{i2}| \Bigg] + \mathcal{O}(\Delta t (\Delta t, h_i^2, k_i^2)).
\end{aligned} \tag{30}$$

We consider now the second equation of (1) and subtract the expression for the exact solution, arriving to the following:

$$\tilde{v}_0^{n+1} = \tilde{v}_0^n \left[1 - \Delta t (1 + m_{00}) \right] + \Delta t a \tilde{u}_0^n + \Delta t \sum_{i=1}^{s} m_{0i} + \mathcal{O}(\Delta t (\Delta t, h_i^2, k_i^2)). \tag{31}$$

Therefore, by the definition of $\tilde{u}^n$ and $\tilde{v}^n$, we get

$$\tilde{v}^{n+1} \leq \Delta t a \tilde{u}^n + \left[\left| 1 - \Delta t (1 + m_{00}) \right| + \Delta t \sum_{i=1}^{s} |m_{0i}| \right] \tilde{v}^n + \mathcal{O}(\Delta t (\Delta t, h_i^2, k_i^2)). \tag{32}$$

For the sake of simplicity let us make

$$\begin{pmatrix} \tilde{u}^{n+1} \\ \tilde{v}^{n+1} \end{pmatrix} \leq \begin{pmatrix} M_{11} & M_{12} \\ M_{21} & M_{22} \end{pmatrix} \begin{pmatrix} \tilde{u}^{n} \\ \tilde{v}^{n} \end{pmatrix}, \tag{33}$$

where M_{21} and M_{22} are clearly given by (32) and M_{11}, M_{12} are given by

$$M_{11} = |1 - \Delta t D m_{00}| + \Delta t D \sum_{i=1}^{s} |m_{i0}| + A_1 \Delta t, \quad M_{12} = \Delta t B_1, \tag{34}$$

for an obvious choice of A_1 and B_1. Then, square matrix in (33) is rewritten as

$$M = \begin{pmatrix} |1 - \Delta t D m_{00}| + \Delta t D \sum_{i=1}^{s} |m_{i0}| + A_1 \Delta t & \Delta t B_1 \\ \Delta t a & |1 - \Delta t (1 + m_{00})| + \Delta t \sum_{i=1}^{s} |m_{i0}| \end{pmatrix}. \tag{35}$$

We consider the $\|\cdot\|_1$ norm as the maximum sum by rows of the elements of M. If it is

$$\|M\|_1 = |1 - \Delta t D m_{00}| + \Delta t D \sum_{i=1}^{s} |m_{i0}| + A_1 \Delta t + \Delta t B_1$$

Hence, $\|M\|_1 < 1$ is equivalent to

$$|1 - \Delta t D m_{00}| < 1 - \Delta t D \sum_{i=1}^{s} |m_{i0}| - A_1 \Delta t - \Delta t B_1,$$

which holds since

$$\Delta t < \frac{2}{D m_{00} + D \sum_{i=1}^{s} |m_{i0}| + A_1 + B_1}.$$

Otherwise, if it holds

$$\|M\|_1 = \Delta t a + |1 - \Delta t (1 + m_{00})| + \Delta t \sum_{i=1}^{s} |m_{i0}|,$$

then,

$$|1 - \Delta t(1 + m_{00})| < 1 - \Delta t a - \Delta t \sum_{i=1}^{s} |m_{i0}|.$$

Last condition is true under the assumptions in Theorem 5.1,

$$\Delta t < \frac{2}{1 + m_{00} + \sum_{i=1}^{s} |m_{i0}| + \Delta t a}.$$

□

6. Numerical study

Lastly, we make use of the GFD scheme (24) to compute the numerical solution of system (4). In order to assess the different convergence cases, we consider constant choices of f, with $r > f$, $r < f$, followed by periodic one. We also include a section of arising patterns that have been found during the numerical simulations, and a final estimate of the order of convergence of the method.

For a greater clarity in representation, despite having considered the method in two spatial dimensions, we only perform the simulations in a one dimensional domain. This allows for simpler visualization, though it could have been done similarly in two or more dimensions.

6.1. The case $r < f$

For this case, we choose the following parameter values

$$D = 0.5, \quad \chi = 2, \quad r = 0.2, \quad a = 1, \quad f(x,t) \equiv 0.5, \tag{36}$$

and initialize the system by taking $u(x,0)$ and $v(x,0)$ as small perturbations of its only non-negative spatially homogeneous steady state, $(0, f)$. As the logistic growth rate r is less than the external source f, we expect the bacterial density u to return to 0 due to the significance of the death rate term $-uv$, given the relative size of the external supply of substance v, which is expected to stabilize at the value of f.

We perform the numerical simulation on $\Omega = (0, 1)$ with a non-homogeneous grid consisting of 19 points unevenly distributed in the interval. As weights we consider $\frac{1}{\text{dist}^4}$, and take a time step of $\Delta t = 1 \cdot 10^{-3}$, which is small enough to grant the convergence of the scheme in the chosen discretization of Ω.

The initial values are taken as

$$u(x,0) = 0.1 \cdot (1 + \cos(3\pi x)), \quad v(x,0) = 0.5 + 0.01 \cdot \sin(8\pi x), \tag{37}$$

as a slight perturbation of the spatially homogeneous steady state $(0, f) = (0, 0.5)$. We solve the equations using scheme (24) until $t = 10$. Figure 1 collects the spatial and temporal evolution of the numerical solutions U and V for this case. The one-dimensional setting allows to represent the temporal dynamics of the solution on moving to the right.

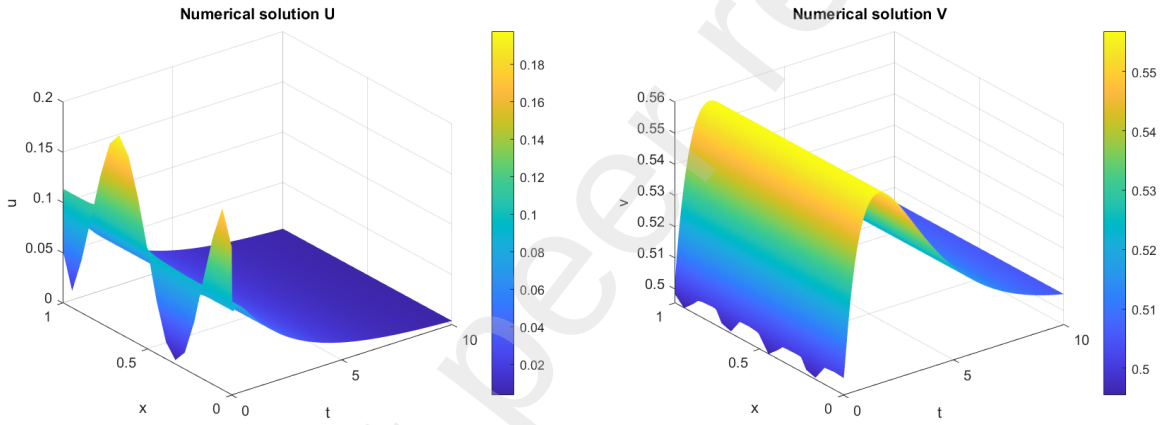

Figure 1: Numerical solutions to system (4) with parameters (36) and initial values (37).

As we can see, in both components u and v, the oscillatory shape of the initial values is rapidly lost caused by the diffusion. In the case of the bacterial population u, the overall high concentrations of the substance —which is constantly supplied at a constant rate higher than the logistic growth—, allow to stop its growth and the solution converges uniformly to zero, the steady state. For v, the supply causes an initial growth of about 5% of its initial value, which is however compensated later on by the decay caused by the term $-v$, converging again to the steady state, given in this case by $f = 0.5$.

For a better representation of these initial dynamics, we plot different time profiles of the solution in Figure 2.

We see that the flattening of the solutions occurs at different time scales, with u still preserving its oscillatory shape at $t = 0.01$. As the dynamics are

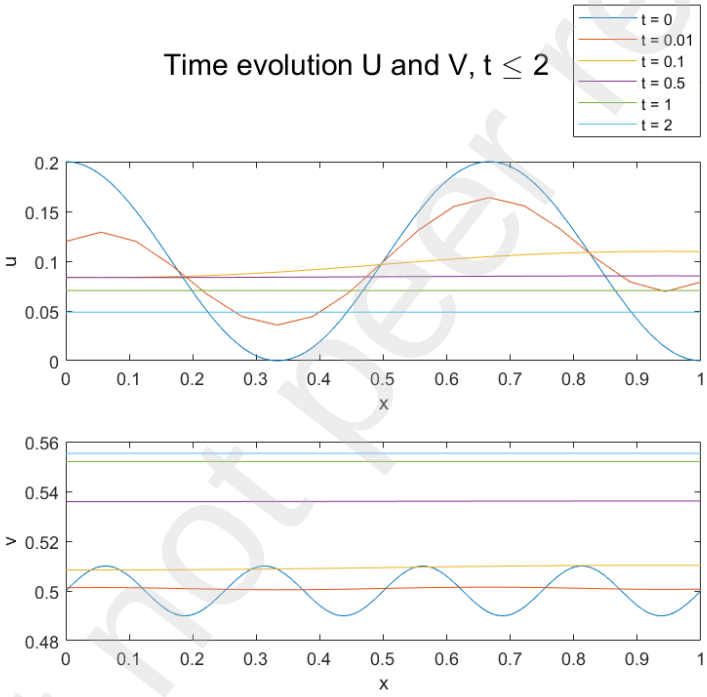

Figure 2: Different time profiles of the solution.

only plotted for $t \leq 2$, we see the growth experimented by v, whereas u only decreases with time.

6.2. The case $r > f$

Now, we explore the case $r > f$, with two different non-negative spatially homogeneous steady states, the previous $(0, f)$ and (u_*, v_*) given in (6). For studying the dynamics close to $(0, f)$, we make use of the same parameters as in Section 6.1 in (36), except for r, which we now take as $r = 1.5$. The initial values $u(x, 0)$ and $v(x, 0)$ are kept as in (37).

As the equilibrium is now unstable, We expect that the drastic change in the logistic growth rate r results in the solution rapidly moving away from $(0, f)$ and converging to (u_*, v_*), which is locally asymptotically stable. Using the same nodes and time step as in the previous case, we obtain the results depicted in Figure 3.

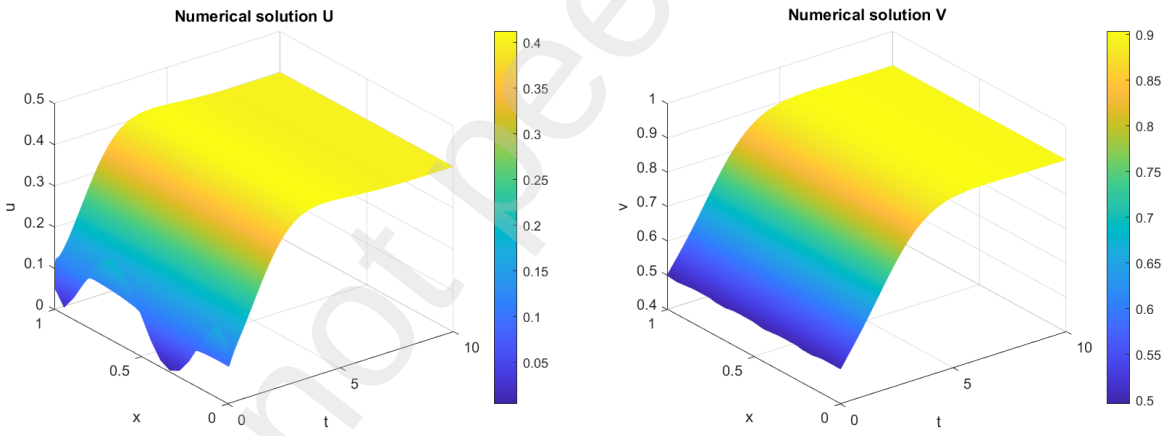

Figure 3: Numerical solution for $r > f$

The results in Figure (3) agree with the expected behavior. Taking into account that r is significantly larger than f, the bacteria rapidly proliferate until the coexistence state u_*, which in this case equals 0.4. As for v, the constant external supply and its production by u allow to overcome the decay and increase its value until converging the equilibrium $v_* = 0.9$.

To analyze this convergence to (u_*, v_*), we represent the time evolution of $||U(., t) - u_*||_{l^\infty(\Omega)}$ and $||V(., t) - v_*||_{l^\infty(\Omega)}$ in Figure (4).

It is interesting to note that both solutions actually achieve their corresponding coordinate of steady state, u_* and v_*, independently at a finite

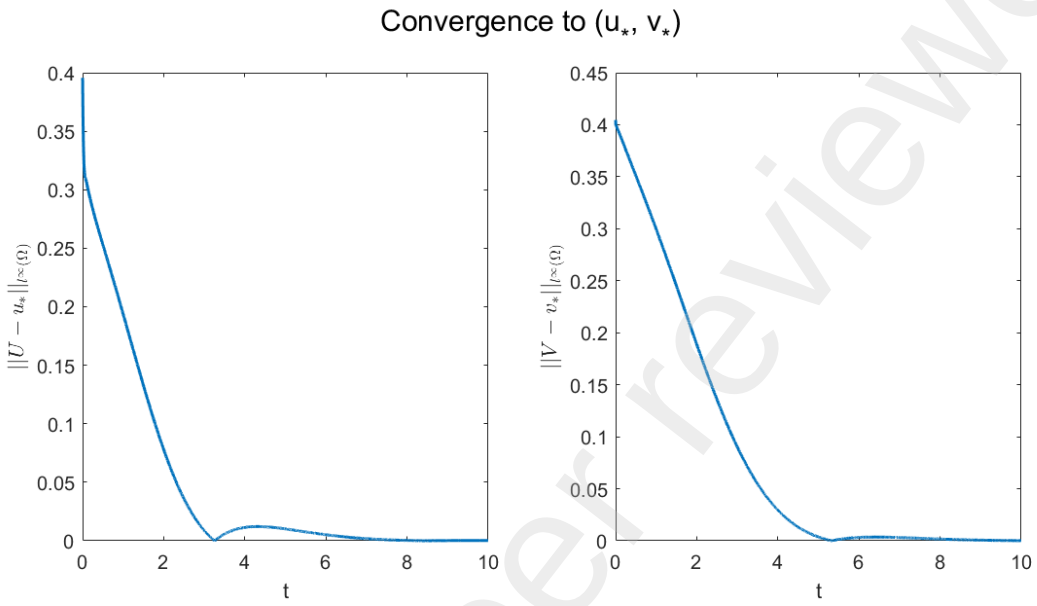

Figure 4: Convergence of the numerical solution (U, V) to the steady state (u_*, v_*).

time. For u, this occurs at approximately $t = 3.16$, while for v it is approximately at $t = 5.24$. However, as the equilibrium values are not reached at the same time, the solution does not remain at the point and instead is slightly perturbed. For larger values of t, we see that both solutions finally converge together to (u_*, v_*).

If we now consider two initial values close to (u_*, v_*), the local asymptotic stability will attract the solution to the equilibrium. For instance, we consider

$$u(x, 0) = u_* + 0.1 \cdot \sin(\pi x), \quad v(x, 0) = v_* + 0.3 \cdot \sin(\pi x). \tag{38}$$

As both initial concentrations have a maximum at $x = 1/2$, given that the chemotaxis is negative, the bacteria will try to avoid the center of the domain, moving to the sides. From then on, we expect diffusion to flatten the shape of the solutions, while returning asymptotically to (u_*, v_*). The results are shown in Figure 5. As in the first case, to better visualize these dynamics, we plot some time profiles of the solution in Figure 6.

As we can see, at $t = 0.01$, in red on the graph, the original shape of u has already changed due to the negative taxis. On the other hand, v still conserves its maximum at $x = 1/2$, as the diffusive time scale is longer. At $t = 0.5$ both solutions have already flattened. For the study of the

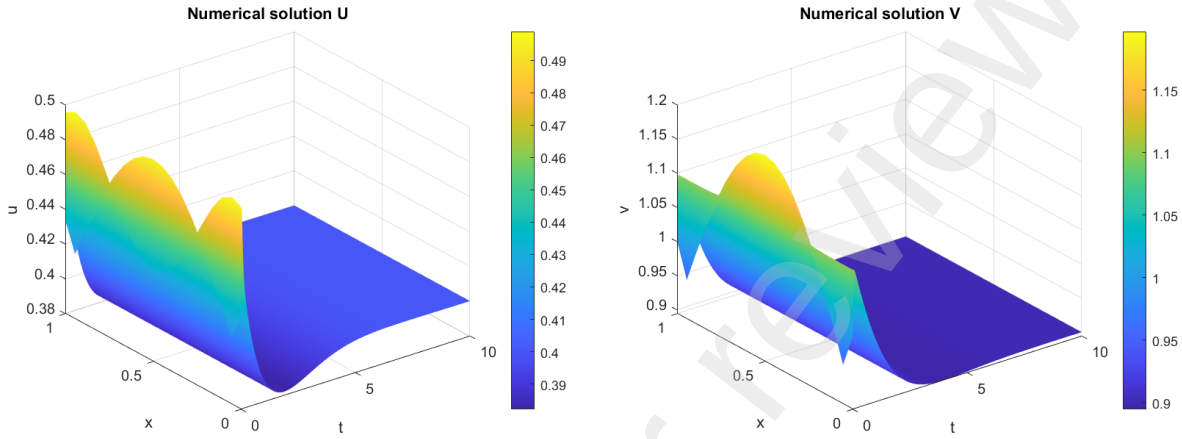

Figure 5: Numerical solutions with initial values (38).

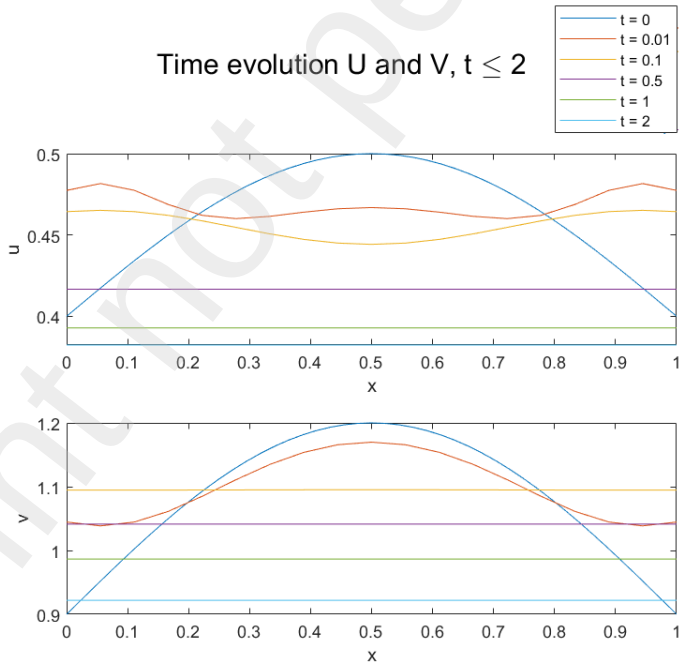

Figure 6: Time profiles of the numerical solution.

convergence, we represent again the time evolution of $||U(.,t)-u_*||_{l^\infty(\Omega)}$ and $||V(.,t)-v_*||_{l^\infty(\Omega)}$ in Figure (7).

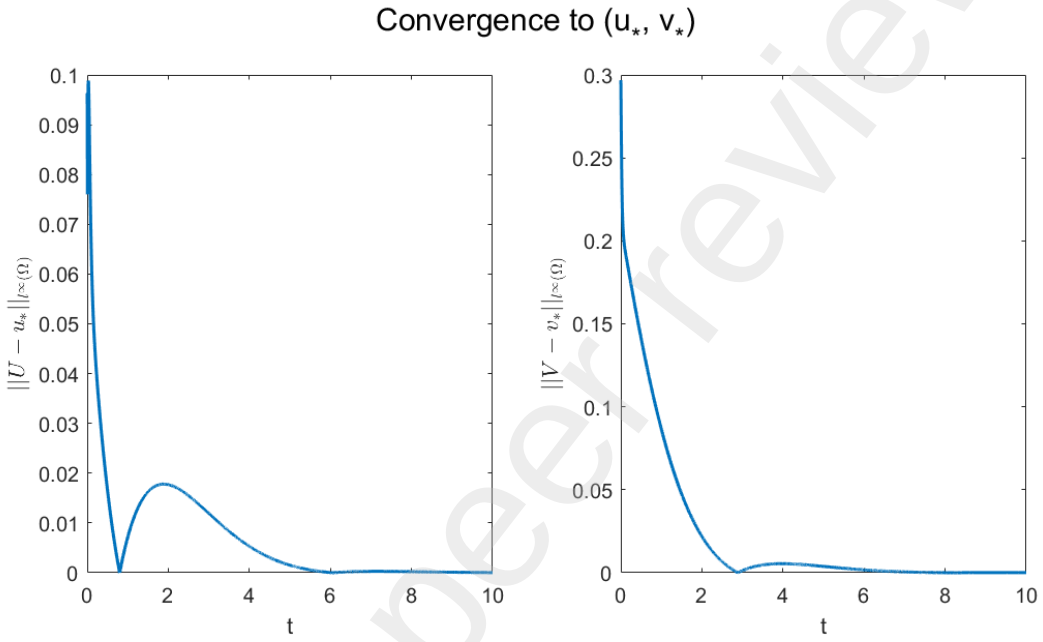

Figure 7: Convergence of the numerical solution (U,V) to the steady state (u_*,v_*).

6.3. Periodicity

Now, we study the case of an asymptotically time-periodic source f, as in Section 3. For this case, we directly consider

$$f(x,t) = 0.5 \cdot [1+\cos(\pi t)], \tag{39}$$

which is itself spatially homogeneous and time-periodic with period $T=2$, so in this case $\hat{f}=f$. The purpose of this section is to analyze the convergence of (u,v), the solution to the original PDE system (4), to $(\tilde{u},\tilde{v})$, the positive periodic solution to the ODE system (10), at every $x\in\Omega$. Recall that the solution $(\tilde{u},\tilde{v})$ is such (positive and periodic) if and only if $(\tilde{u}_0,\tilde{v}_0)$ are taken as in (15), and (12) and $r>r_{\min}$, the threshold value.

To achieve this, we start by computing u_0 and v_0 with our choice of $\hat{f}$. Following (12), we have

$$\tilde{v}_0 = \frac{1}{e^T-1}\int_0^T \hat{f}(s)e^s\,ds = \frac{1}{2}\left(1+\frac{1}{\pi^2+1}\right), \tag{40}$$

and with it

$$\tilde{v}(t) = \frac{1}{2}\left(1 + \frac{1}{\pi^2+1}\big(\pi\sin(\pi t) + \cos(\pi t)\big)\right). \tag{41}$$

Before determining $\tilde{u}_0$, we obtain the threshold value $r_{\min}$, given in (18). In this case, we directly have $r_{\min} = 1/2$.

We perform two numerical simulations, one with $r > r_{\min}$, with which we expect (u, v) to converge in every point to $(\tilde{u}, \tilde{v})$, and another one with $r < r_{\min}$, in which the resulting solution may be oscillatory, due to the periodicity of f, but not periodic.

First we take for instance

$$r = 0.75 > r_{\min}, \quad D = 0.5, \quad \chi = 2, \tag{42}$$

and for this case we had set $a = 0$. With these parameter values we can calculate $\tilde{u}_0$, the periodic solutions to the ODE system $(\tilde{u}, \tilde{v})$, and the solutions to the PDE system (u, v). As initial values we take

$$u(x, 0) = 0.2 + 0.1 \cdot \sin(\pi x), \quad v(x, 0) = 0.3 \cdot \sin(\pi x). \tag{43}$$

The evolution of u and v is depicted in Figure 8, where the asymptotic periodicity can be observed.

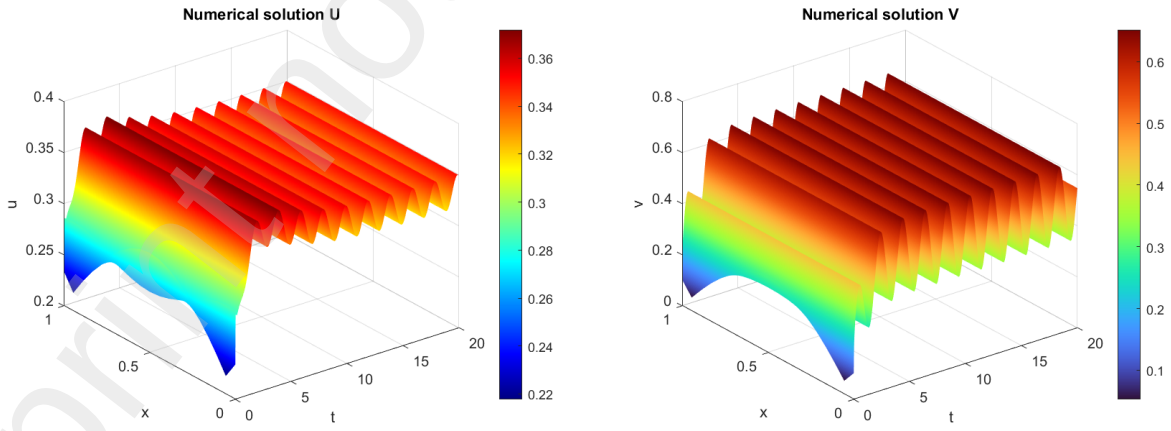

Figure 8: Numerical solution to system (4) with parameters (42) and initial values (43).

To better analyze the convergence to $(\tilde{u}, \tilde{v})$, we take the fixed coordinate

$x = 1/2$ and plot in Figure 9 the time evolution of $u(1/2, t)$ and $v(1/2, t)$, along with $\tilde{u}(t)$ and $\tilde{v}(t)$.

Given the shape of the initial bacterial and substance distributions, both having a maximum precisely at $x = 1/2$, as in previous cases the bacterial population flee the center of the domain, and thus $u(1/2, t)$ experiments a sudden decrease in the first instants. Diffusion causes $v(1/2, t)$ to also decrease initially, albeit less intensely. From there on, the logistic dynamics of the bacteria and the external supply of the substance boost the growth of both u and v. With r being sufficiently large, the bacteria soon grow until reaching a first maximum at around $t = 2$. The death term $-uv$ prevents a greater increase of the population, that ends up converging to $\tilde{u}$, being sufficiently close to it soon after $t = 10$. The convergence of v to $\tilde{v}$ is faster, having very similar values already at $t = 4$.

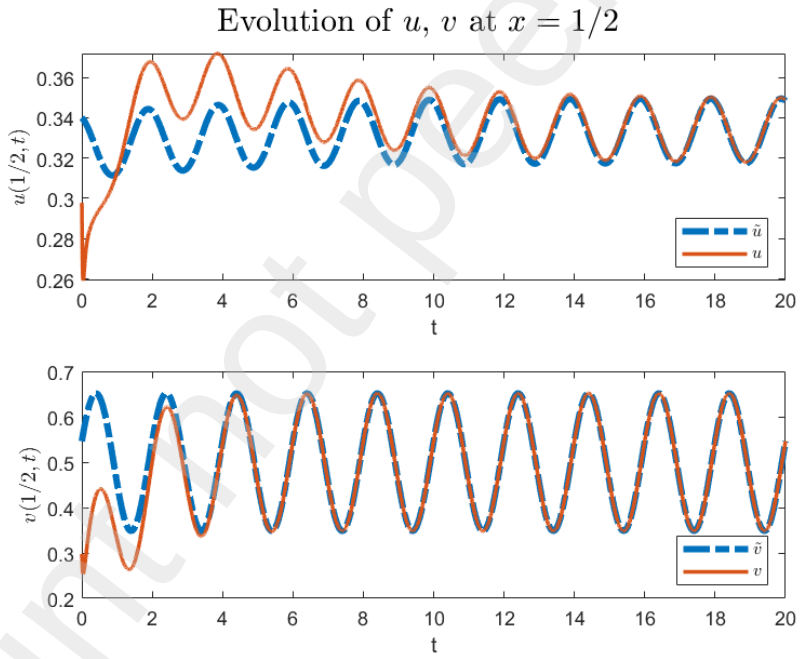

Figure 9: Convergence of (u, v) to $(\tilde{u}, \tilde{v})$ at $x = 1/2$.

Secondly, we simulate the system with a value of r below $r_{\min}$, where no positive periodic solution $(\tilde{u}, \tilde{v})$ to the ODE system (10) exists. Taking now $r = 0.4$ with the remaining parameters as in (42), f as in (39), and the same initial values (43), we compute the numerical solutions represented in Figure

10.

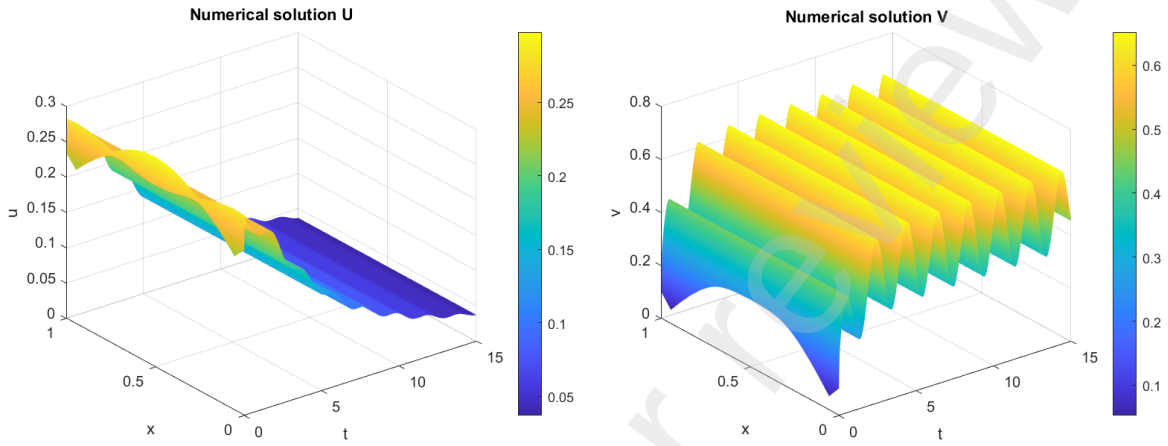

Figure 10: Numerical solution with $r = 0.4 < r_{\min}$, remaining parameters from (42) and initial values (43).

Here we see that instead of converging to a time-periodic solution, u suffers an oscillating decay, with the logistic dynamics being insufficient to increase the bacterial population, given the significance of the death term $-uv$, as v is indeed large enough. However, v does appear to converge to a periodic solution, which we verify by representing again the time evolution at the the fixed $x = 1/2$ in Figure 11.
With respect to the case $a > 0$, no explicit conditions can be derived for the existence of positive periodic solutions to the associate ODE system, as the second equation is no longer uncoupled. However, it can be proven [12] that if there exists, then (u, v) converge again in time to $(\tilde{u}, \tilde{v})$, the corresponding positive periodic solutions, at all $x \in \Omega$.

To show an example, we consider f as in (39) and the same initial values given in (43), taking

$$r = 1, \quad a = 1, \quad D = 0.5, \quad \chi = 2. \tag{44}$$

The numerical solutions are represented in Figure 12, again with the time evolution at $x = 1/2$ in Figure 13.
In this case, the high value of r allows for a rapid initial growth of the bacterial population, which is however then compensated by the also very high concentrations of the substance, almost reaching 0.9. As we see, the

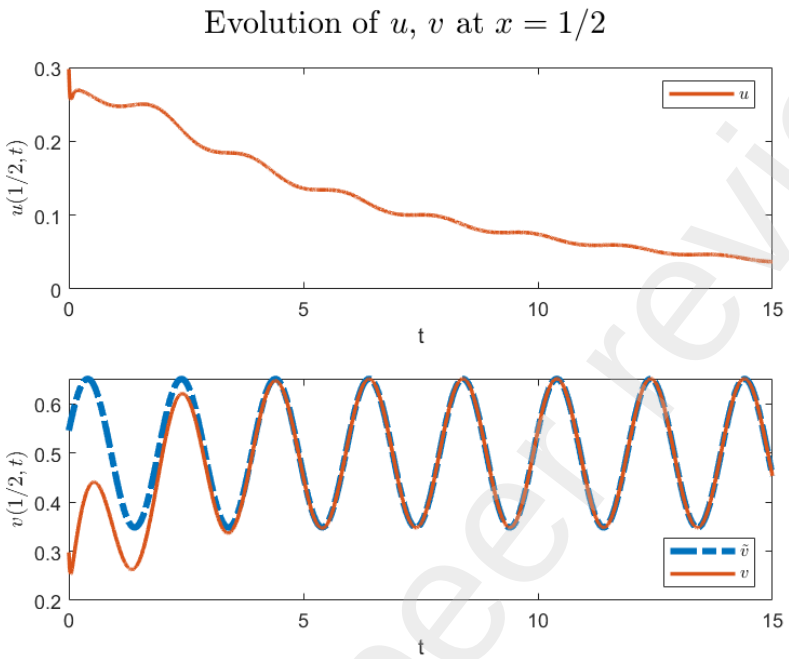

Figure 11: Time evolution of u and v at $x = 1/2$

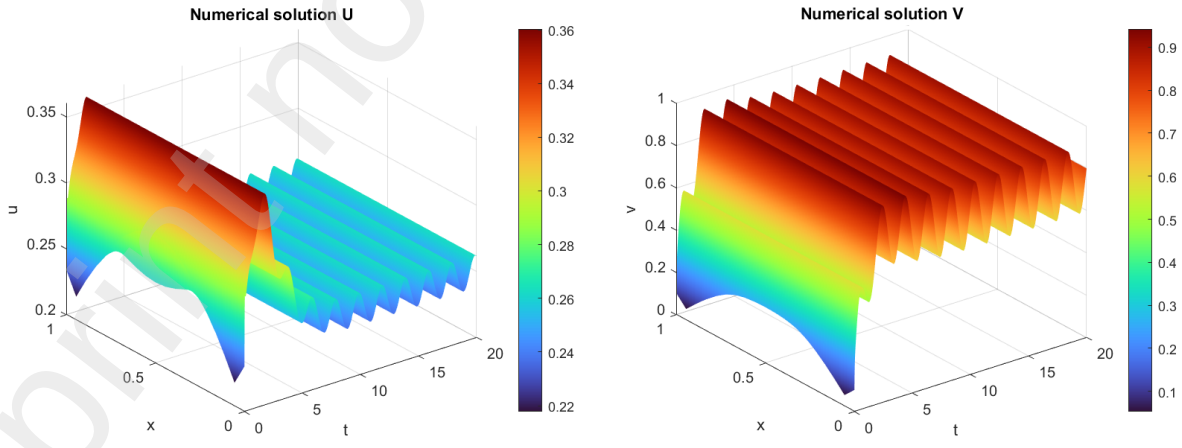

Figure 12: Numerical solution with parameters (44) and initial values (43).

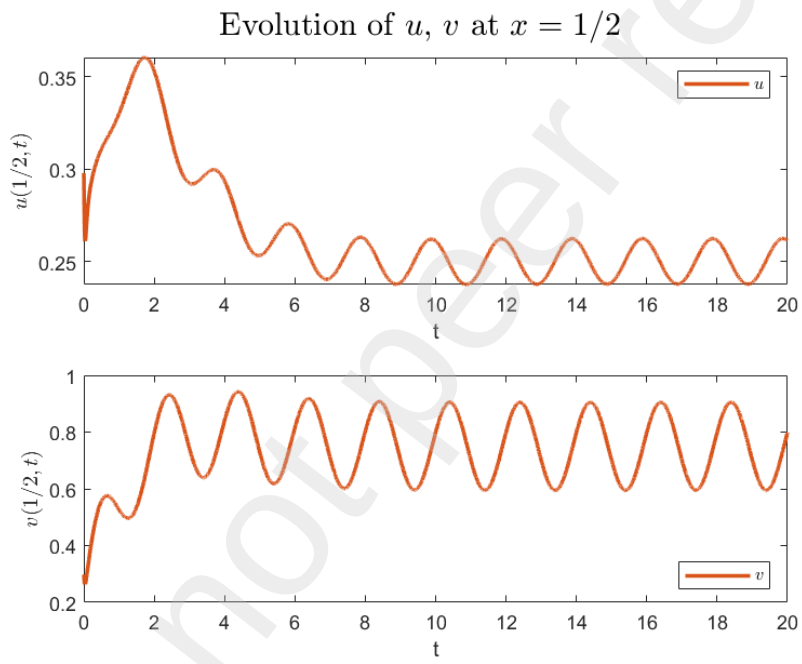

Figure 13: Convergence to periodic solutions at $x = 1/2$.

solutions then converge to the corresponding solutions $(\tilde{u}, \tilde{v})$ of the associated ODE system.

6.4. Arising patterns

Lastly, we devote this section to show some spatial patterns that can be generated by our system (4) under certain parameter configurations. A wide range of patterns in a simple chemotaxis system in one spatial dimension is described in detail in [22].

To obtain meaningful results, we consider a longer domain, in this case $\Omega = (-\pi, \pi)$ and first take the following parameters

$$D = 0.1, \quad \chi = 9, \quad r = 1, \quad a = 1, \quad f(x,t) \equiv 0. \tag{45}$$

Notice that in this case diffusion is almost two orders lower than chemotaxis. As initial values, we consider a small perturbation around $(u^*, v^*) = (0.5,\ 0.5)$, given by

$$u(x,0) = u^* = 0.5, \quad v(x,0) = v^* + 0.01 \cdot \sin(8x) = 0.5 + 0.01 \cdot \sin(8x). \tag{46}$$

The numerical solution until $t = 15$ is represented in Figure 14. As we can see, focusing on the bacterial density, there are emerging clusters of bacteria with high population densities, while other parts of the domain remain almost empty.

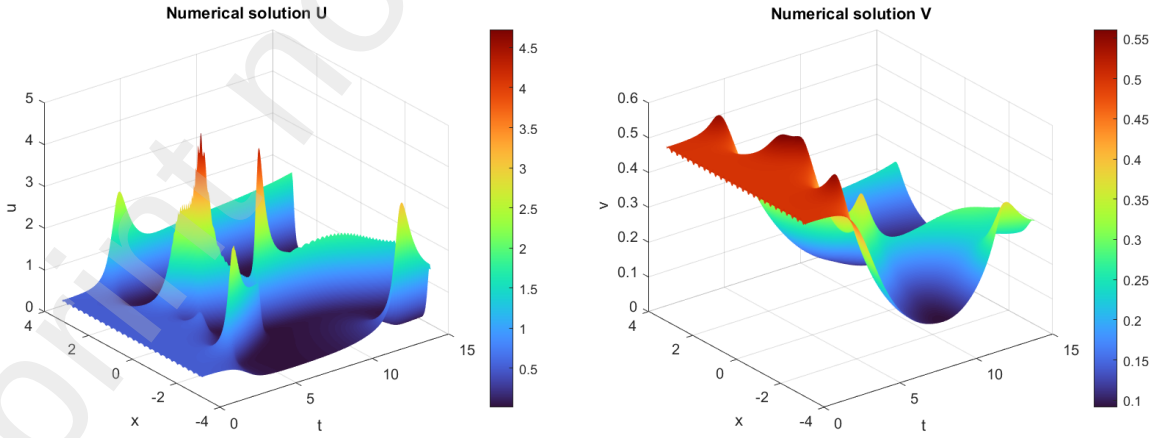

Figure 14: Numerical solution to system (4) with parameter values (45) and initial values (46).

To better visualize these merging and emerging clusters, on Figure 15 we represent various time profiles of the solution u, as well as a vertical view of the left image on Figure 14.

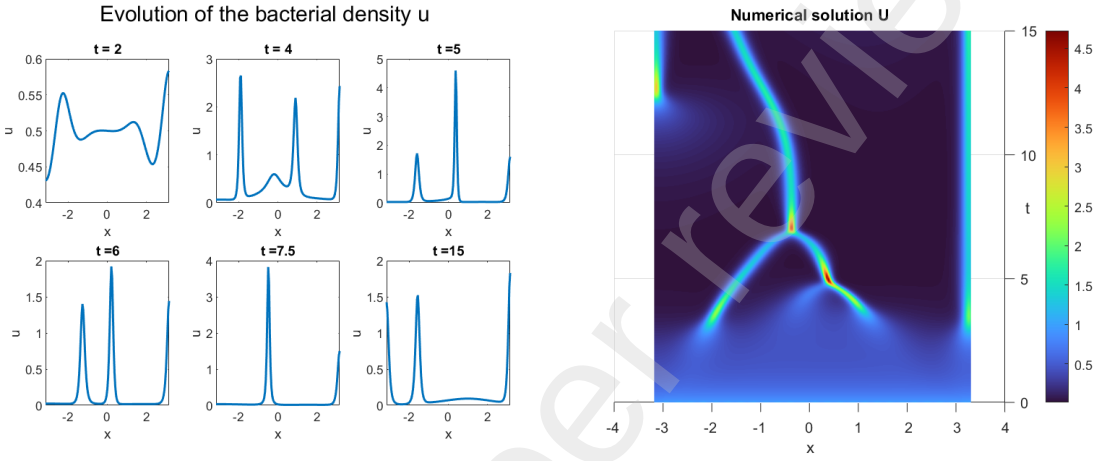

Figure 15: Evolution of the u component of the solution

We see that until $t = 2$, the solution remains close to u^*, with the different small aggregations being bounded between 0.4 and 0.6. However, from then on, certain peaks start to emerge, as we see at $t = 4$. The greater concentrations are located around $x = -2$, $x = -0.5$, $x = 1$ and at the boundary $x = \pi$. The two middle ones end up merging into one, which happens shortly before $t = 5$, which can be better visualized in the right diagram. The remaining two aggregates that are not located in the boundary merge again before $t = 7.5$. Notice that at this moment, the bacterial density is nearly 4 at the center of the bacterial cluster, much greater than the carrying capacity of the logistic model, which is normalized to 1. This leads to a decrease in the population density. We see in the right image that a third peak emerges at the left boundary $x = -\pi$ after $t = 12$, which can be seen in the final profile at $t = 15$, where all densities are already below 2.

Similar patters seem to arise when considering a larger domain. For instance, in Figure 16 we consider $\Omega = (-\frac{3\pi}{2}, \frac{3\pi}{2})$, with the same relation of parameters as in (45), except for $\chi = 6$. The results are represented once again in a vertical view, only for u.

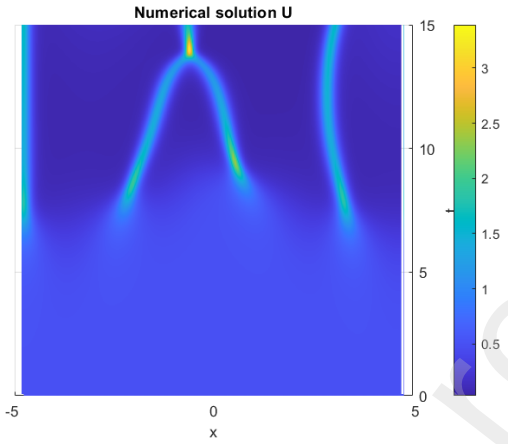

Figure 16: Numerical solution to system (4) with parameter values (45) and initial values (46).

Though at the initial stages, until $t = 7$ approximately, the solution does not present great spatial heterogeneity, four bacterial clusters emerge. First, one near the left boundary; two at the center of the domain, which end up merging into one before $t = 15$, and a last one at the right side of Ω. At a lower value of χ compared to the previous case, these aggregations do not achieve the same high densities as before, never reaching 3.5 in this case, whereas previously the maximum value was slightly below 5.

6.5. Numerical order of convergence

As a final remark, in this last subsection we numerically estimate the order of convergence (O.C.) of the proposed scheme. We compare an artificial solution over three different meshes with 10, 19 and 37 nodes, yielding the results in Table 1, where we see that the estimated order of convergence is close to its actual value, 2.

Number of nodes	l^∞ norm of the error	O.C.
10	0.00114	-
19	$5.4183 \cdot 10^{-4}$	2.103
37	$2.0811 \cdot 10^{-4}$	2.603

Table 1: Maximum error in l^∞ for three different meshes and numerical order of convergence.

7. Conclusions

Throughout this paper we have presented and analyzed a model describing the interaction between a biological species and a chemical substance, represented by equations (4). The system accounts for cell motility, negative chemotaxis and logistic growth for the bacteria, as well as the lethality caused by the substance and an external supply of it.

The local stability of the spatially homogeneous steady states was studied in Section 2, obtaining two different equilibria, $(0, f)$ and (u_*, v_*), given in (6), the former being positive only if $r > f$. In this case, as the growth rate of the logistic model is greater than the external supply, the state $(0, f)$ is unstable, whereas the coexistence state, (u_*, v_*) is locally asymptotically stable. On the contrary, if $r < f$, the state $(0, f)$ is locally asymptotically stable, as any bacterial growth would be compensated by the supply of the chemical.

For an asymptotically time-periodic source function f, the associated ODE system was studied in Section 3 for the case $a = 0$. The explicit solution of the second component of the system, $\tilde{v}$, allowed to obtain the initial data for which the system exhibits periodic behavior. Moreover, a threshold value for r with respect to $\hat{f}$ was determined in (18), which guarantees the existence of a positive periodic solution to the ODE system if $r > r_{\min}$ and the initial values are taken as in (12) and (15). Under such hypothesis, the original PDE system converges in time to this periodic solution.

The remaining sections were devoted to a numerical study of the problem. Section 4 introduces the Generalized Finite Difference Method, which is used to compute the numerical solution to the system. The numerical scheme used was presented in Section 5 in (24), obtaining a bound for the time step that ensures its convergence in Theorem 5.1.

The linear stability of the steady states, as well as the convergence to periodic solutions were verified numerically in Section 6. For the linear stability, the cases $r < f$ and $r > f$ were considered, showing the corresponding numerical solution in Figures 1, 3 and 5. Regarding the periodicity, a case with $r > r_{\min}$ was simulated, obtaining the convergence represented in Figure 9, as well as one with $r > r_{\min}$ where u experimented an oscillating decay, as could be seen in Figure 11. Lastly, some final remarks on pattern formation in the system and the convergence of the method were given, in Figure 15 and Table 1, respectively.

Declaration of competing interest

The authors declare that they have no known competing financial interests or personal relationships that could have appeared to influence the work reported in this paper.

Data availability

No data was used for the research described in the article.

Acknowledgments

This work was supported by Project PID2022-141114NB-I00 by Ministerio de Ciencia e Innovación (Spain) and by Grant FPU23/03170 (F.H-H.) from the Spanish Ministry of Science, Innovation and Universities.

References

[1] Bai X, Winkler M. *Equilibration in a fully parabolic two-species chemotaxis system with competitive kinetics.* Indiana Univ. Math. J., **65** (2),553–583, (2016).

[2] N. Bellomo, A. Bellouquid, Y. Tao, M. Winkler. Toward a mathematical theory of Keller-Segel models of pattern formation in biological tissues. *Math. Model. Methods Appl. Sci.*, 25, 1663–1763, (2015).

[3] Benito J. J., García A., Gavete L., Negreanu M., Ureña F., Vargas A. M. *On the numerical solution to a parabolic-elliptic system with chemotactic and periodic terms using Generalized Finite Differences*. Engineering Analysis with Boundary Elements, **113**, 181-190, (2020). DOI: 10.1016/j.enganabound.2020.01.002.

[4] Benito J. J., García A., Gavete L., Negreanu M., Ureña F., Vargas A. M. *Solving a fully parabolic chemotaxis system with periodic asymptotic behavior using Generalized Finite Difference Method*. Applied Numerical Mathematics, **157**, 356-371, (2020).

[5] Benito J. J., García A., Gavete L., Negreanu M., Ureña F., Vargas A. M. *Solving a chemotaxis-haptotaxis system in 2D using Generalized Finite Difference Method*. Computers & Mathematics with Applications, **80** (5), 762-777, (2020).

[6] Benito J. J., García A., Gavete L., Negreanu M., Ureña F., Vargas A. M. *On the convergence of the generalized finite difference method for solving a chemotaxis system with no chemical diffusion.* Comp. Part. Mech. (2020). https://doi.org/10.1007/s40571-020-00359-w.

[7] Benov L, Fridovich I. *Escherichia coli exhibits negative chemotaxis in gradients of hydrogen peroxide, hypochlorite, and N-chlorotaurine: products of the respiratory burst of phagocytic cells.* Proc. Natl. Acad. Sci. USA. **93 (10), 4999-5002**, (1996).

[8] Cundliffe E, Demain AL. *Avoidance of suicide in antibiotic-producing microbes.* J Ind Microbiol Biotechnol. 37(7):643-72, (2010).

[9] Drangeid A. K. *The principle of linearized stability for quasilinear parabolic evolution equations.* Nonlinear Anal. 13 1091–1113, (1989).

[10] Herrero-Hervás F., Negreanu M., Vargas A. M., *Convergence of a meshless numerical method for a chemotaxis system with density-suppressed motility,* Computers & Mathematics with Applications 148, 293-301, (2023).

[11] Herrero-Hervás F. *An explicit–implicit Generalized Finite Difference scheme for a parabolic–elliptic density-suppressed motility system.* Journal of Computational and Applied Mathematics, 446, (2024).

[12] Herrero-Hervás F., Negreanu M. *Asymptotics and periodic dynamics in a negative chemotaxis system with cell lethality*, Preprint (2025)

[13] Hillen T, Painter K. J.. A users guide to PDE models for chemotaxis. *Journal of Mathematical Biology*, 58, 183–217, (2009).

[14] Horstmann D. *From 1970 until present: the Keller-Segel model in chemotaxis and its consequences*, Jahresbericht der Deutschen Mathematiker-Vereinigung. **105** (3), 103-165, (2003).

[15] Imlay J.A., Linn, S. *Bimodal pattern of killing of DNA-repair-defective or anoxically grown Escherichia coli by hydrogen peroxide* J Bacteriol. **166** (2), (1986).

[16] Keller E.F., Segel L.A. *Initiation of slime mold aggregation viewed as an instability.* J. Theoret. Biol. **26**, 399-415, (1970).

[17] Keller E.F., Segel L.A. *A model for chemotaxis.* J. Theoret. Biol. **30**, 225-234, (1971).

[18] Lancaster P., Salkauskas K. *Curve and surface fitting*, Ed. Academic Press, (1986).

[19] Mizukami M. *Boundedness and asymptotic stability in a two-species chemotaxis-competition model with signal-dependent sensitivity.* Discrete and Continuous Dynamical Systems - B. **22** (6) 2301-2319, (2017).

[20] Negreanu M., Vargas A.M. *On a fully parabolic chemotaxis system with source term and periodic asymptotic behavior.* Zeitschrift für angewandte Mathematik und Physik. **71**, 65, (2020).

[21] Negreanu M., Tello, J.I., Vargas A.M. *Continuous and discrete periodic asymptotic behavior of solutions to a competitive chemotaxis PDEs system.* Communications in Nonlinear Science and Numerical Simulation. **95**, 105592, (2021).

[22] Painter K.J, Hillen T. *Spatio-temporal chaos in a chemotaxis model.* Physica D, **240**, 363-375, (2011).

[23] Ravindra Kumar S., Imlay J.A. *How Escherichia coli tolerates profuse hydrogen peroxide formation by a catabolic pathway.* J Bacteriol. **195** (20), 4569-79, (2013)

[24] Seaver L.C., Imlay J.A. *Hydrogen Peroxide Fluxes and Compartmentalization inside Growing Escherichia coli,* J Bacteriol. **183** (24), (2001).

[25] Stinner C., Tello J.I., Winkler M. *Competitive exclusion in a two-species chemotaxis model.* Journal of Mathematical Biology **68** (7), 1607-1626, (2014).

[26] Tello J.I., Winkler M. *Stabilization in a two-species chemotaxis system with logisitc source. N*onlinearity **25**, 1413-1425, (2012).

[27] Uhl L, Gerstel A, Chabalier M, Dukan S. *Hydrogen peroxide induced cell death: One or two modes of action?* Heliyon, **1** (4), (2015)

[28] Vargas A.M., *Finite difference method for solving fractional differential equations at irregular meshes*, Mathematics and Computers in Simulation. **193**, 204-216, (2022).

[29] Zhang Q., Li Y. *Global solutions in a high-dimensional two-species chemotaxis model with Lotka–Volterra competitive kinetics*. Journal of Mathematical Analysis and Applications **467** (1), 751-767, (2018).